Modelling of Whale Optimization Algorithm with Deep Learning for Skin Cancer Diagnosis on Dermoscopic Images

[1,*]**Vijay Arumugam R.**, [2]**Saravanan S.**
[1]Department of Computer Science, Government Arts and Science College,
Manalmedu, Tamilnadu.
vijaynew@gmail.com
[2]Department of Computer and Information Science, Annamalai University,
Annamalai Nagar, Chidambaram, Tamilnadu.
aucissaran@gmail.com

Abstract—Skin cancer diagnoses through the analysis of dermoscopy images have undergone a revolutionary change with the incorporation of advanced Machine Learning (ML) approaches. By using contemporary models such as Convolutional Neural Network (CNN) and Deep Learning (DL) structures, this technique allows automated and accurate detection of malignant and benign skin tumours. This model learns intricate patterns and features directly from the image, which allows them to distinguish between different types of skin tumours based on colour, texture, and structural characteristics. This manuscript presents the Whale Optimization Algorithm with Deep Learning for Skin Cancer Diagnoses on Dermoscopy Images (WOADL-SCDDI) technique. The objective of the WOADL-SCDDI method is to analyze the Dermoscopic images for classifying and recognizing skin tumours. In the proposed WOADL-SCDDI technique, median filtering-based preprocessing and SegNet-based segmentation are involved. In addition, the WOADL-SCDDI technique offers a ResNet50 model for feature extraction with WOA-based hyperparameter tuning. Finally, Quasi Recurrent Neural Network (QRNN) model can be applied for skin tumour recognition and classification process. A comprehensive set of simulations have been conducted to highlight the better efficiency of the WOADL-SCDDI technique. The accomplished outcomes portrayed the improvements of the WOADL-SCDDI method compared to existing DL models.

Keywords- Dermoscopy; Skin cancer; Machine learning; Whale optimization algorithm; Deep learning;

I. INTRODUCTION

Skin carcinoma is a majorly prevalent familiar carcinoma all over the world. It is challenging for the skin specialists to diagnose skin tumours from dermoscopic images [1]. In many cases, pathology and biopsy analysis is required for diagnosing cancer. Earlier investigations established computer-based structures for identifying the images of skin tumours [2]. Previous to 2016, these techniques are dependent on the traditional ML approach that needed the segmentation of cancer from the neighbouring skin region in an image, and then the extraction of valuable factors from the cancerous region [3]. These behaviours contain the colour, texture, and shape of the lesion. Lastly, the factors are provided in a classifier for diagnosing tumours [4]. This technique has been complex due to it is hard to determine and extract features, which can be beneficial for identifying cancer [5].

Various approaches are developed for automatically diagnosing tumour infected skin areas [6]. Initially, the handcrafted factors-based method is presented for tumour identification. ML and Artificial Intelligence (AI) technologies have concreted the approach for novel probabilities for assistive

diagnosing in the biomedicine and medical sector [7]. Generally, CNN-based techniques are extensively utilized in medical imaging for segmentation and classification applications [8]. With current developments in hardware and software technologies, DL can be developed as a robust mechanism for feature learning. Feature engineering is referred to as the process to define and extract features by a human professional, which has complex and time-taking tasks [9]. DL technique eradicates the requirement for feature engineering due to it is automated to learn and extract valuable features from fresh information [10]. DL approach has developed various domains specifically Computer Vision (CV). The DL algorithm established major accomplishments in current research.

This manuscript offers the design of a Whale Optimization Algorithm with Deep Learning for Skin Cancer Diagnosis on Dermoscopy Imaging (WOADL-SCDDI) technique. In the proposed WOADL-SCDDI technique, median filtering-based preprocessing, and SegNet-based segmentation are involved. In addition, the WOADL-SCDDI technique offers a ResNet50 model for feature extraction with WOA-based hyperparameter tuning. Finally, Quasi Recurrent Neural Network (QRNN) model can be applied for skin tumour recognition and

2018

_____

classification process. A comprehensive set of simulations have been conducted to highlight the better efficiency of the WOADL-SCDDI method.

II. RELATED WORKS

Zhou et al. [11] developed a novel method termed as Multi-Site Cross-Organ Calibration based-DL (MuSClD) that utilizes WSIs of *off-target* organs for standardization produced at a similar region as *on-target* organs. The author determined employing an off-target organ from the assessment region for calibrating trained data, the domain transfer amongst trained and tested information can be alleviated. Bassel et al. [12] developed an approach that depends upon the stacking of classifiers 3-fold for classifying benign and melanoma skin tumours. The method is trained in 3 levels by KNN, RF, SVM, NN, LR, and DL approaches with 1000 skin images with the classifications of benign and melanoma. The major feature extraction is implemented by employing the VGG16, Resnet50, and Xception techniques. In [13], the authors introduced 2 new fusion CNN algorithms with an SVM technique at the output layer to classify dermoscopic imageries for both melanoma and benign cancers. This features extraction through the CNN algorithm is integrated and provided to the SVM technique for classifying. The class labels attained from skilled dermatologists have been utilized as the conditions for estimating the efficiencies of developed techniques.

Adla et al. [14] developed an automatic DL with a layer of class attention-based CAD algorithm. Tsallis entropy-based segmenting has been used for the diagnosis of the affected cancerous regions. Moreover, a DLCAL-based feature extracting process has been exploited to extract the factors from the segmented lesions by CapsNet as well as CAL and Adagrad optimization. Eventually, Swallow Swarm Optimizer (SSO) technique-based Convolution Sparse AE (CSAE) termed SSO-CSAE has been implemented for classification. In [15], introduced a new DL-IoHT method determined for the classification of skin cancer. Automatic features were extracted from images employing various pre-trained models such as SqueezeNet, Inception V3, VGG19, and ResNet50 that are provided into Fully Connected (FC) for classifying the skin malignant and benign cells. Besides, the developed approach is entirely incorporated with an IoHT technique.

Alwakid et al. [16] suggested a DL method to extract a cancerous zone with accuracy. Firstly, the image was improved by employing Enhanced Super-Resolution Generative Adversarial Networks (ESRGAN) technique. Secondly, segmentation can be utilized for segmenting ROI from the whole image. The authors applied data augmentation for rectifying the data dissimilarity. This image can be further examined with a CNN and an adapted form of Resnet-50 for classifying skin cancers.

III. THE PROPOSED MODEL

In this manuscript, the design and construction of the automated WOADL-SCDDI method is offered on Dermoscopy images. The key purpose of the WOADL-SCDDI method is to analyze the Dermoscopic images for classifying and recognizing skin tumours. In the proposed WOADL-SCDDI technique, median filtering-based preprocessing, SegNet-based segmentation, ResNet50-based feature extracting, QRNN and WOA based classification and tuning process. Fig. 1 describes the entire process of the WOADL-SCDDI technique.
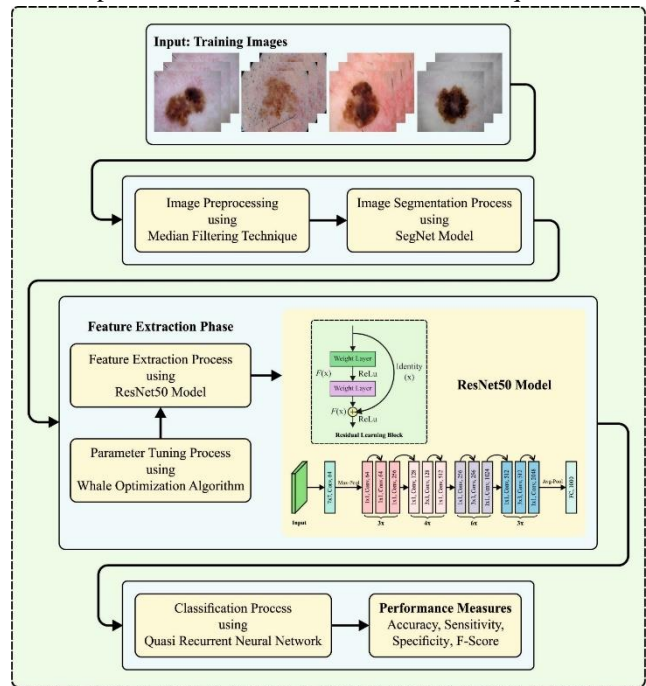
Figure 1. Overall flow of the WOADL-SCDDI model

A. Image Preprocessing and Segmentation

In the presented WOADL-SCDDI technique, MF-based preprocessing, and SegNet-based segmentation processes. MF-based preprocessing is an underlying method used to prepare and enhance images, especially in the fields of CV and image processing [17]. Noise and small irregularities within the image can be reduced effectively by employing this method. MF replaces the pixel values with the median values of its neighbouring pixels within a specified window or neighbourhood. This method is particularly helpful in scenarios where outliers or salt-and-pepper noise are present, as it aids fine details and preserves edges while efficiently suppressing unwanted variation. For segmentation, the SegNet model is applied with 13 convolution layers in every encoding and decoding network, subsequently, the softmax layer is accountable for possibilities for each class per pixel. At last, the segmented outputs generated by the class are existing in all the pixels. Max-pooling indices (rather than applying skip connection in UNet) of the factor maps in the encoding system are recorded and used in its decoding network for higher

2019

_____

outcomes, making it highly effective. Compared to other semantic segmentation networks, SegNet has enormous benefits such as requiring less memory, compactness in size, and more availability to be trained.

$$s(x_i) = \frac{e^{x_i}}{\sum_{j=1}^{n} e^{x_j}} \qquad (1)$$

In Eq. (1), x indicates the output vector, i represents the range of 0 to $n-1$, and n refers to the number of classes.

If the images with a dimension of MxN are given into the initial layer of the encoder, then the activation map of $(m+1)^{th}$ decoding layer is represented in Eq. (3), and the activation maps of $(m+1)^{th}$ layers of the encoder are shown in Eq. (2).

$$x_{m+1} = \{MAX[ReLU(conv_m\{x_m\} + b_m)]\} \qquad (2)$$
$$y_{m+1} = NORM[conv_m\{US(y_m) + b_m\}] \qquad (3)$$

In the equation, y_m represents the activation maps of the mth decoding layer, x_m indicates the activation maps of mth encoding layer, b_m shows the learned bias of mth layer, $ReLU[\cdot]$ denotes the activation function, MAX $[\cdot]$ shows the Maxpooling function, US $(\cdot)$ shows the upsampling, $NORM$ refers to the batch normalization, and $conv\{\cdot\}$ denotes the convolution operation.

B. Feature Extraction by employing Optimum ResNet Technique

At this stage, the ResNet50 architecture is used for the feature extraction process. ResNet is another basic CNN deployed as the backbone in several CV applications [18]. He et al. in 2015 originally developed a ResNet with 150 layers, to resolve the gradient waning problems. The ResNet architecture is a skip connection, or shortcut path, from before the present layers; this skip connection adds an identity function from prior layers, therefore present layer performs as a prior layer. This development minimizes the gradient disappearing problems in DNN. The ResNet50 model, with 5 phases of repetitive block. Every phase comprises "Conv" and "Identity" blocks. Conv block consists of 3 convolution layers of 1x1 (n), 3x3 (n), and 1x1 (4n) filter sizes (where n = amount of filters), correspondingly. A shortcut connection links the inputs and outputs of the "Conv" block through the batch normalization and convolution (stride 2) layer. Likewise, the "Identity" block uses three successive convolution layers of 1x1 (n), 3x3 (n), and 1x1 (4n) filter size (stride = 1 for each layer). Lastly, the ResNet50 model contains 12 Identity blocks (36 layers), 1 convolution layer (7x7), 4 Conv blocks (12 layers), and 1 FC layer.

The WOA is employed for the optimum selection of hyperparameter of the ResNet50 architecture in this article. WOA is a metaheuristic optimization technique stimulated by the hunting behaviours of whales and adjusting parameters for discovering the optimum solution [19]. This algorithm is easy to implement and has a straightforward concept. Moreover, it easily bypasses local optimum and shows faster convergence. First, this approach generates a population and computes the fitness score of all the individuals like other metaheuristic optimization techniques. Next, it traverses the existing population to search for individuals with better fitness. Later, the individual location was upgraded in the population by mimicking the whale behaviours, involving surrounding prey, BubbleNet attacking, and searching for targets. It continues to search for optimum individuals and update individual positions until the maximal amount of iterations is attained as the population progresses to the following generation. P and A values define an individual whale updating its location:

$$P = random(0,1) \qquad (4)$$
$$R_1 = random(0,1) \qquad (5)$$
$$a = 2 - 2 * \frac{t}{T_{max}} \qquad (6)$$
$$A = 2 * a * R_1 - a \qquad (7)$$

Where t, and τ_{max} portrays the present and maximum iteration numbers and this can be mathematically modelled as follows:

$$R_2 = random(0,1) \qquad (8)$$
$$C = 2 * R_2 \qquad (9)$$
$$l = random(-1,1) \qquad (10)$$

If $P < 0.5$ and $|A| < 1$, then individuals update their location by surrounding prey. The computation equation is given below, where $X(t)$ indicates the location of the existing individual, $X(t+1)$ shows the updated location of the individuals, and X_{best} denotes the existing optimum individuals:

$$D_1 = |C * X_{best} - X(t)| \qquad (11)$$
$$X(t+1) = X_{best} - A * D_1 \qquad (12)$$

If $P < 0.5$ and $|A| \geq 1$, then the individual will find prey, and the whale arbitrarily chooses a position to force itself further than the prey, thus allowing a global searching process:

$$rand = randint [1, whale - num] \qquad (13)$$
$$D_2 = |C * X_{rand} - X(t)| \qquad (14)$$
$$X(t+1) = X_{rand} - A * D_2 \qquad (15)$$

If $P \geq 0.5$, then update the location by BubbleNet attacking. In the meantime, the whale gets closer to the in a spiral movement for capturing the food. Thus, it is formulated as follows:

$$D_3 = |X_{best} - X(t)| \qquad (16)$$
$$X(t+1) = X_{best} + D_3 * e^{b*l} * cos(2\pi l) \qquad (17)$$

In Eq. (21), D_3 shows the distance between the existing and the optimum individuals. b refers to the coefficient that signifies the spiral shape of whales as 1.

Algorithm 1: The pseudocode of the WOA approach

_____

Input:

G: the maximal iteration

b: a constant to define the shape of a logarithmic spiral

n: the whale population count

Output: Optimum individual X_{best} and fitness value f_g

Initialization of whale population $X_i (i = 1,2, … , n)$

Compute the fitness value of every individual

While $(t < G)$

For all the individuals

Update $a, A, C, 1, P$

If1 $(P < 0.5)$

If2 $(|A| < 1)$

X_i update the location by surrounding prey

Else if2 $(|A| \geq 1)$

X_i update the location by looking for prey

End if2

Else if1 $(P \geq 0.5)$

X_i update the location by BubbleNet attacking

End if1

End for

Check whether the individuals exceed the limit and eliminate them

Compute the fitness values of the overall individuals

Update the existing optimum individual X_{best} and its fitness f_g

End while

Return X_{best}, f_g

Fitness selection is a major element of the WOA technique. Solution encoding is applied for measuring the aptitude of the solution candidate. Here, the accuracy values are the most important condition employed for developing a FF.

$$Fitness = \max (P) \qquad (18)$$

$$P = \frac{TP}{TP + FP} \qquad (19)$$

Where TP and FP depicts the true and false positive values.

C.   Image Classification

Lastly, the QRNN model is exploited for the classification method. QRNN is a hybrid NNs of LSTM and CNN, incorporating both advantages [20]. Like CNN, QRNN is highly parallelizable based on LSTM. Each layer of QRNN incorporates 2 seed mechanisms, based on the pooling and convolution layers. Fig. 2 depicts the infrastructure of QRNN. Both layers completely permit similar computation: the convolution layer assists in parallelization through spatial dimensional (i.e., sequence size) and mini-batch; the pooling layer assists in parallelized via mini-batch and feature size. The equation of the QRNN component is described as:

$$\hat{x}_t = tanh(W * X_t)$$
$$f_t = \sigma(W_f * X_t)$$
$$o_t = \sigma(W_o * X_t) \qquad (20)$$

$$c_t = f_t \odot c_{t-1} + (1 - f_t) \odot \hat{x}_t$$
$$h_t = o_t \odot tanh(c_t)$$

In Eq. (20), $X_\tau \in \mathbb{R}^{k \times n}$ shows the input sequence of kn-dimension vectors $x_{t-\kappa+1}, ., x_t$.
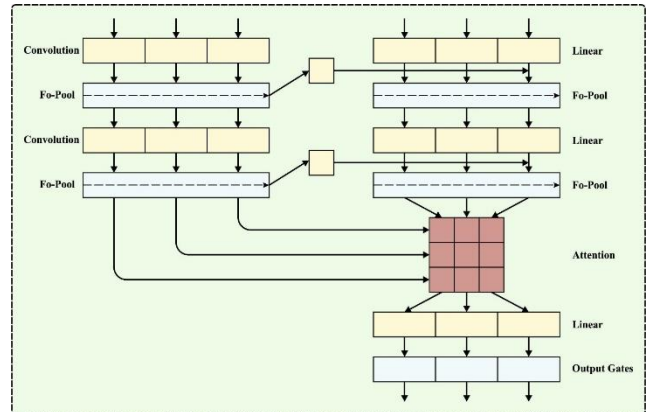
Figure 2.   Architecture of QRNN

The operator $*$ shows the mask convolution besides the timestep size. W, W_f and W_o show the convolution filter bank in $\mathbb{R}^{d \times n \times k}$, and k portrays the filter width. The main 3 formulas are the convolutional part of QRNN, and this convolution function creates m-dimension sequence $\hat{x}_t$, f_t, and o_t. The operator $\odot$ means element-wise multiplication. The last 2 terms are the pooling part of QRNN, whereas the element-wise gate performs in the LSTM unit. The function is parallelized in one matrix-matrix multiplication as:

$$u^T = \begin{pmatrix} W \\ W_f \\ W_o \end{pmatrix} [X_{k-1}, X_k, … , X_{L+k-1}] \qquad (21)$$

In Eq. (21), $U \in R^{L \times 3d}$, d, and $L = T - k + 1$ represents the outcome matrix, hidden state neurons number; and the sequence input length.

IV. PERFORMANCE VALIDATION

The investigational analysis of the WOADL-SCDDI technique is assessed on ISIC 2017 and HAM10000 datasets. The ISIC2017 dataset includes 2000 instances with three classes and is depicted in Table 1.

TABLE I.   DATASET DESCRIPTION ON ISIC 2017 DATASET

Class	Label	Sample Numbers
Melanoma	Class-1	374
Seborrheic Keratosis	Class-2	254
Nevus	Class-3	1372
Overall Samples		**2000**

Fig. 3 exhibits the classifying results of the WOADL-SCDDI approach on the ISIC2017 database. Figs. 3a-3b describes the confusion matrix presented by the WOADL-SCDDI approach at

2021

70:30 of the TR set/TS set. The outcome indicated that the WOADL-SCDDI technique has detected and classified all 3 classes. Simultaneously, Fig. 3c shows the PR analysis of the WOADL-SCDDI technique. The output specified that the WOADL-SCDDI technique has attained the highest PR value of 3 classes. Lastly, Fig. 3d determines the ROC curve of the WOADL-SCDDI model. The output showed that the WOADL-SCDDI model has given an output in promising outputs with the highest values of ROC in the 3 classes.
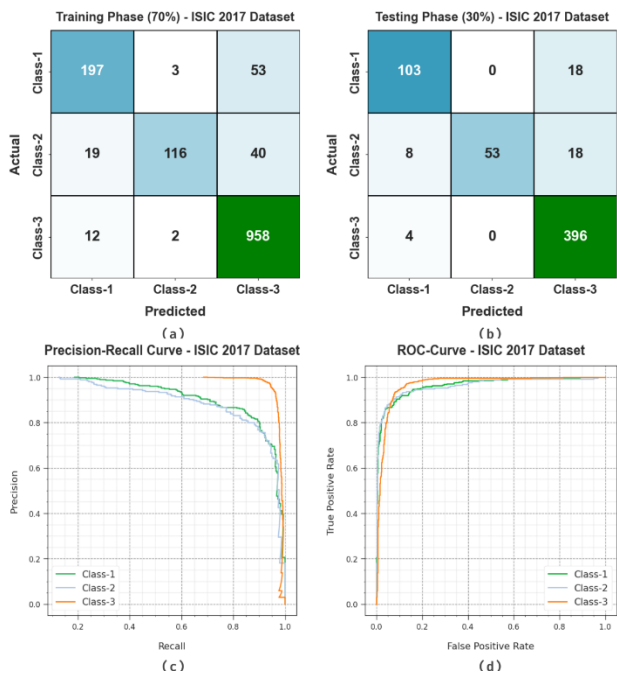
Figure 3. Performances on ISIC2017 dataset (a-b) Confusion matrices, (c-d) Curves of PR and ROC

TABLE II. SKIN CANCER RECOGNITION OUTCOME OF WOADL-SCDDI TECHNIQUE ON ISIC2017 DATASET

Class	$Accu_y$	$Sens_y$	$Spec_y$	F_{Score}	MCC
TR set (70%)					
Class-1	93.79	77.87	97.30	81.91	78.33
Class-2	95.43	66.29	99.59	78.38	77.53
Class-3	92.36	98.56	78.27	94.71	81.82
Average	**93.86**	**80.90**	**91.72**	**85.00**	**79.23**
TS set (30%)					
Class-1	95.00	85.12	97.49	87.29	84.22
Class-2	95.67	67.09	100.00	80.30	79.94
Class-3	93.33	99.00	82.00	95.19	85.04
Average	**94.67**	**83.74**	**93.16**	**87.59**	**83.07**

In Table 2 and Fig. 4, the skin cancer recognition performance of the WOADL-SCDDI algorithm is tested on the ISIC2017 dataset. The experimental outcomes inferred that the WOADL-SCDDI method properly recognizes three classes.

With a 70% TR set, the WOADL-SCDDI technique provides an average $accu_y$, $sens_y$, $spec_y$, F_{score}, and MCC of 93.86%, 80.90%, 91.72%, 85%, and 79.23% correspondingly. At the same time, with a 30% TS set, the WOADL-SCDDI method provides an average $accu_y$, $sens_y$, $spec_y$, F_{score}, and MCC of 93.86%, 80.90%, 91.72%, 85%, and 79.23% correspondingly.
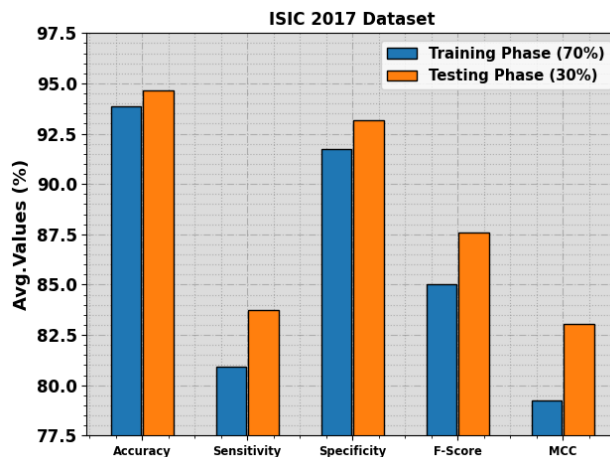
Figure 4. Average of WOADL-SCDDI technique on ISIC2017 dataset

Fig. 5 shows the training accuracy TR_accu_y and VL_accu_y of the WOADL-SCDDI technique on the ISIC2017 dataset. The TL_accu_y is determined by the assessment of the WOADL-SCDDI technique on the TR dataset while the VL_accu_y is calculated by evaluating the achievement on a discrete test data. The outputs exhibit that TR_accu_y and VL_accu_y increase with an upsurge in epochs. As a result, the performance of the WOADL-SCDDI technique gets to improve on the dataset of TR and TS with a growth in the epochs number.

Figure 5. $Accu_y$ curve of WOADL-SCDDI technique on ISIC2017 dataset

In Fig. 6, the TR_loss and VR_loss outcomes of the WOADL-SCDDI technique on the ISIC2017 dataset are shown. The TR_loss determines the fault amid the initial and anticipated values on TR data. The VR_loss represent the performance measure of the WOADL-SCDDI method on

_____

discrete validation data. The outputs indicate that the TR_loss and VR_loss tend to minimize with rising epochs. It exemplifies the augmented achievement of the WOADL-SCDDI method and its ability for generating precise classification. The mitigated TR_loss and VR_loss value illustrates the superior achievement of the WOADL-SCDDI technique in capturing patterns and relationships.
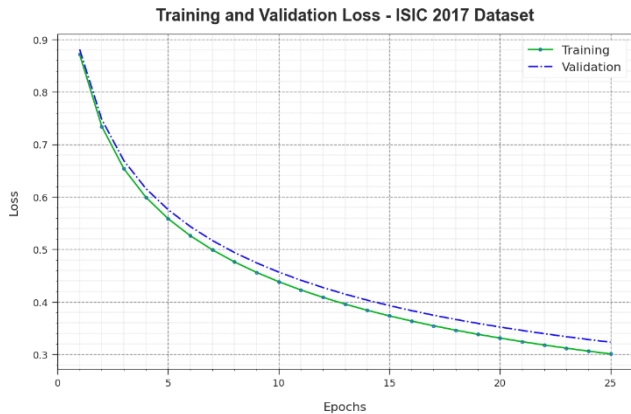
Figure 6.   Loss curve of WOADL-SCDDI technique on ISIC2017 dataset

For ensuring the improvised results of the WOADL-SCDDI technique, relative research is conducted on the ISIC2017 dataset, as given in Table 3 and Fig.7. The investigational value highlighted that the MobileNet model accomplishes worse results. Next to that, the NB, KELM, MSVM, and DenseNet169 models obtain moderately improved performance. Along with that, the MAFCNN-SCD technique reaches considerable outcomes. Nevertheless, the WOADL-SCDDI technique accomplishes superior performance with maximum $accu_y$, $sens_y$, $spec_y$, and F_{score} of 94.67%, 83.74%, 93.16%, and 87.59% correspondingly.

TABLE III.   COMPARISON OUTCOME OF THE WOADL-SCDDI METHOD WITH OTHER TECHNIQUES ON THE ISIC2017 DATASET

Methods	$Accu_y$	$Sens_y$	$Spec_y$	F_{Score}
WOADL-SCDDI	94.67	83.74	93.16	87.59
MAFCNN-SCD	92.22	77.07	88.67	83.05
NB	89.77	74.70	84.02	81.37
KELM	88.04	77.03	84.49	83.2
MSVM	87.15	75.44	83.19	81.45
MobileNet	85.03	74.17	87.98	81.18
DenseNet_169	89.42	76.83	86.28	83.27
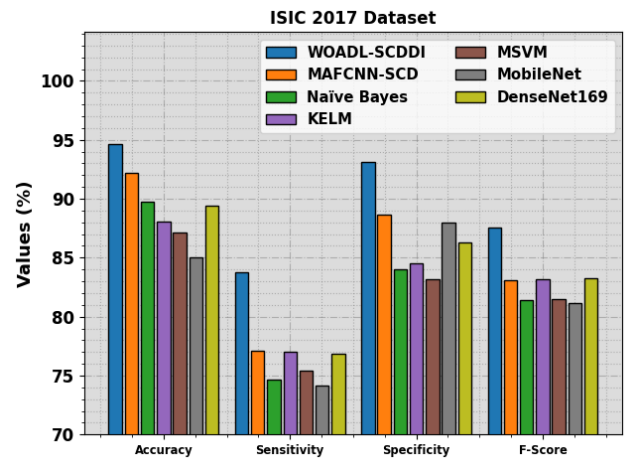
Figure 7.   Relative output of WOADL-SCDDI technique on the ISIC2017 dataset

Table 4 demonstrates the detailed description of the HAM10000 dataset has 10082 samples with 7 class labels such as Actinic Keratoses (AKIEC), Basal Cell Carcinoma (BCC), Benign Keratosis (BKL), Dermatofibroma (DF), Melanocytic Nevus (NV), Melanoma (MEL), and Vascular (VASC).

TABLE IV.   DATASET DESCRIPTION ON HAM10000 DATASET

Class Name	Sample Numbers
AKIEC	327
BCC	541
BKL	1099
DF	155
NV	6705
MEL	1113
VASC	142
Overall Samples	10082

Fig. 8 exhibits the classifying outputs of the WOADL-SCDDI system on the HAM10000 dataset. Figs. 8a-8b exemplifies the confusion matrix presented by the WOADL-SCDDI technique at 70:30 of the TR set/TS set. The outcome indicated that the WOADL-SCDDI method has detected and categorized all 7 classes. As well, Fig. 8c shows the PR examination of the WOADL-SCDDI technique. The outcome showed that the WOADL-SCDDI method has attained the highest PR performance in the 7 classes. Finally, Fig. 8d depicts the ROC analysis of the WOADL-SCDDI method. The output showed that the WOADL-SCDDI technique has given an output in promising results with high values of ROC in 7 classes.
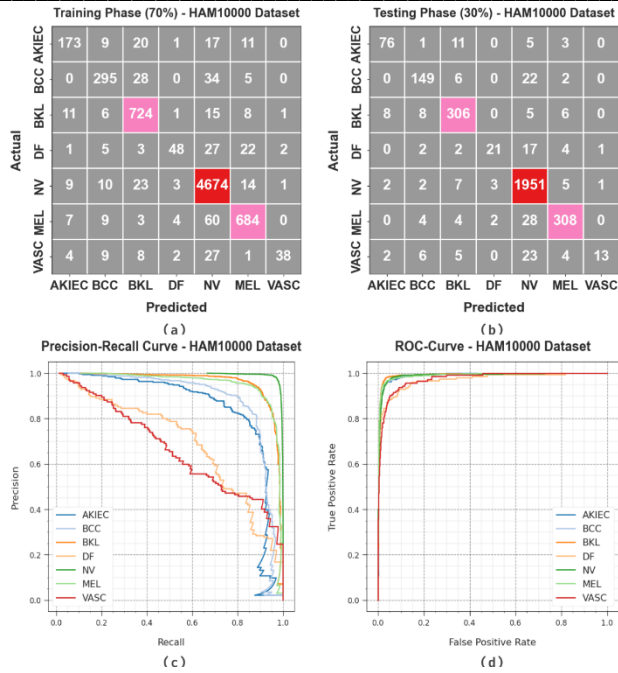
Figure 8.   Fig. 8 Performances on HAM10000 dataset (a-b) Confusion matrices, (c-d) Curves of PR and ROC

In Table 5 and Fig. 9, the skin cancer recognition outputs of the WOADL-SCDDI technique are experimented on the HAM10000 dataset. The outputs inferred that the WOADL-SCDDI technique properly recognizes three classes. With 70% TR set, the WOADL-SCDDI technique provides an average $accu_y$, $sens_y$, $spec_y$, F_{score}, and MCC of 98.30%, 75.14%, 98.36%, 79.78%, and 79.41% correspondingly. At the same time, with a 30% TS set, the WOADL-SCDDI method provides an average $accu_y$, $sens_y$, $spec_y$, F_{score}, and MCC of 98.10%, 73.07%, 98.12%, 77.42%, and 77.44% correspondingly.

TABLE V.   SKIN CANCER RECOGNITION OUTCOME OF WOADL-SCDDI TECHNIQUE ON HAM10000 DATASET

Class	$Accu_y$	$Sens_y$	$Spec_y$	F_{Score}	MCC
TR set (70%)					
AKIEC	98.72	74.89	99.53	79.36	78.85
BCC	98.37	81.49	99.28	83.69	82.86
BKL	98.20	94.52	98.65	91.94	90.97
DF	98.99	44.44	99.84	57.49	59.71
NV	96.60	98.73	92.25	97.50	92.27
MEL	97.96	89.18	99.03	90.48	89.35
VASC	99.22	42.70	99.94	58.02	61.86
Average	**98.30**	**75.14**	**98.36**	**79.78**	**79.41**
TS set (30%)					
AKIEC	98.94	79.17	99.59	82.61	82.15
BCC	98.25	83.24	99.19	84.90	83.99
BKL	97.95	91.89	98.70	90.80	89.66
DF	98.98	44.68	99.83	57.53	59.64
NV	96.03	98.99	90.51	97.02	91.27

MEL	97.95	89.02	99.10	90.86	89.73
VASC	98.61	24.53	99.93	38.24	45.69
Average	**98.10**	**73.07**	**98.12**	**77.42**	**77.44**
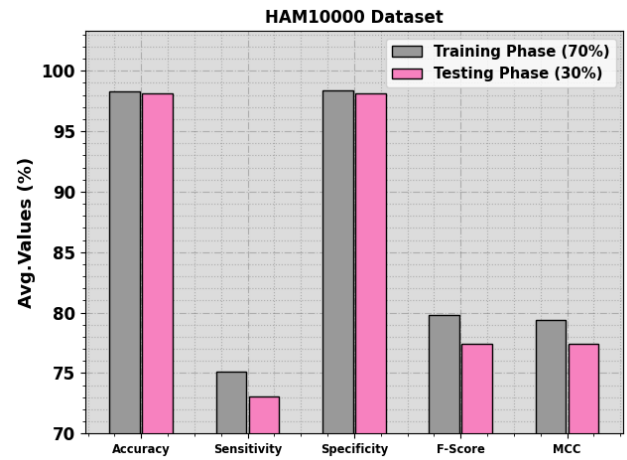
Figure 9.   Average of WOADL-SCDDI technique on HAM10000 dataset

Fig. 10 shows the training accuracy TR_accu_y and VL_accu_y of the WOADL-SCDDI methodology on the HAM10000 dataset. The TL_accu_y is determined by the assessment of the WOADL-SCDDI methodology on TR data while the VL_accu_y is assessed by evaluating the achievement on a discrete test data. The results exhibit that TR_accu_y and VL_accu_y increase with an upsurge in epochs. As a result, the performance of the WOADL-SCDDI technique gets to improve on the TR and TS dataset with a growth in the number of epochs.
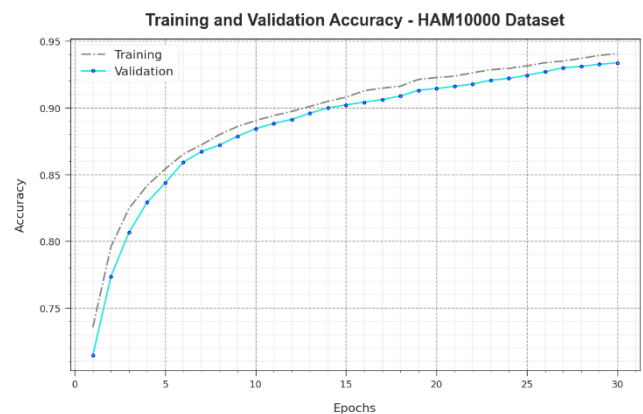
Figure 10. $Accu_y$ curve of WOADL-SCDDI technique on HAM10000 dataset

In Fig. 11, the TR_loss and VR_loss outputs of the WOADL-SCDDI methodology on the HAM10000 dataset are shown. The TR_loss defines the fault amid the initial and anticipated values on TR data. The VR_loss represent the performance measure of the WOADL-SCDDI methodology on discrete validation data. The results indicate that the TR_loss and VR_loss tend to decrease with rising epochs. It exemplifies the augmented achievement of the WOADL-SCDDI approach

2024

and its ability for generating precise classification. The mitigated TR_loss and VR_loss values illustrate the enhanced achievement of the WOADL-SCDDI approach in capturing patterns and relationships.
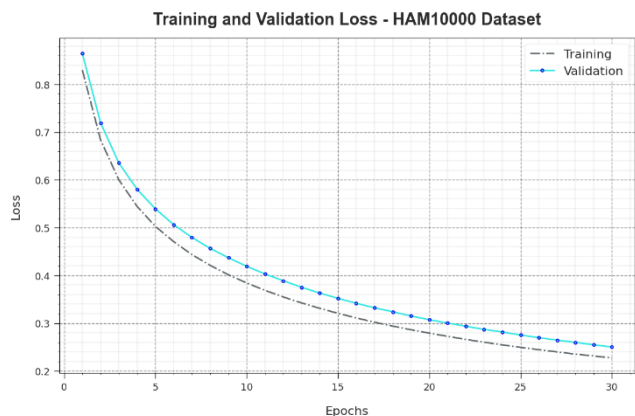
Figure 11. Loss curve of WOADL-SCDDI model on HAM10000 dataset

For ensuring the improvised results of the WOADL-SCDDI technique, a relative examination is made on the dataset namely HAM10000, as given in Table 6 and Fig. 11. The experimental values highlighted that the MobileNet model obtains worse outcomes. In addition to that, the NB, KELM, MSVM, and DenseNet169 techniques attain moderately better performance. Along with that, the MAFCNN-SCD method attains considerable outcomes. Nevertheless, the WOADL-SCDDI technique accomplishes superior performance with high $accu_y$, $sens_y$, $spec_y$, and F_{score} of 98.30%, 75.14%, 98.36%, and 79.78% subsequently.

The experimental results conclude that the WOADL-SCDDI technique gains improved skin cancer classification performance.

TABLE VI. RELATIVE OUTPUT OF WOADL-SCDDI TECHNIQUE WITH OTHER APPROACHES ON THE HAM10000 DATASET

Methods	$Accu_y$	$Sens_y$	$Spec_y$	F_{Score}
WOADL-SCDDI	98.30	75.14	98.36	79.78
MAFCNN-SCD	92.22	72.07	88.67	75.05
NB	89.77	74.20	84.02	76.07
KELM	88.04	73.03	84.49	75.20
MSVM	87.15	73.44	83.19	74.45
MobileNet	85.03	74.17	87.98	76.18
DenseNet_169	89.42	72.83	86.28	77.02

V. CONCLUSION

In this manuscript, the design and development of the automated WOADL-SCDDI approach is offered on Dermoscopy images. The major aim of the WOADL-SCDDI approach is to analyze the Dermoscopic images for the recognition and classification of skin tumours. In the presented WOADL-SCDDI technique, median filtering-based preprocessing, SegNet and ResNet50 based segmentation and feature extraction, WOA and QRNN based hyperparameter tuning, and classification. Besides, the WOADL-SCDDI technique offers a ResNet50 model for feature extraction with WOA-based hyperparameter tuning. Finally, the QRNN technique can be applied to the process of skin cancer recognition and classification. A comprehensive set of simulations have been conducted to highlight the better efficiency of the WOADL-SCDDI method. The accomplished outcomes portrayed the improvements of the WOADL-SCDDI method compared to existing DL models.

REFERENCES

[1] Albraikan, A.A., Nemri, N., Alkhonaini, M.A., Hilal, A.M., Yaseen, I. and Motwakel, A., 2023. Automated Deep Learning Based Melanoma Detection and Classification Using Biomedical Dermoscopic Images. *Computers, Materials & Continua*, *74*(2).

[2] Lafraxo, S., Ansari, M.E. and Charfi, S., 2022. MelaNet: an effective deep learning framework for melanoma detection using dermoscopic images. *Multimedia Tools and Applications*, *81*(11), pp.16021-16045.

[3] Soujanya, A. and Nandhagopal, N., 2023. Automated Skin Lesion Diagnosis and Classification Using Learning Algorithms. *Intelligent Automation & Soft Computing*, *35*(1).

[4] Attique Khan, M., Sharif, M., Akram, T., Kadry, S. and Hsu, C.H., 2022. A two-stream deep neural network-based intelligent system for complex skin cancer types classification. *International Journal of Intelligent Systems*, *37*(12), pp.10621-10649.

[5] Ahmed, S., Abiduzzaman, M.D., Rajib, M.H., Rahaman, R., Hussain, S., Rashid, H.B., Wadud, A.H. and Bhuiya, T.A.U.H., 2023, February. Human Skin Diseases Detection and Classification using CNN. In *2023 International Conference on Electrical, Computer and Communication Engineering (ECCE)* (pp. 1-6). IEEE.

[6] Nawaz, M., Mehmood, Z., Nazir, T., Naqvi, R.A., Rehman, A., Iqbal, M. and Saba, T., 2022. Skin cancer detection from dermoscopic images using deep learning and fuzzy k-means clustering. *Microscopy research and technique*, *85*(1), pp.339-351.

[7] Manoj, S.O., Abirami, K.R., Victor, A. and Arya, M., 2023. Automatic Detection and Categorization of Skin Lesions for Early Diagnosis of Skin Cancer Using YOLO-v3-DCNN Architecture. *Image Analysis & Stereology*, *42*(2), pp.101-117.

[8] Alam, T.M., Shaukat, K., Khan, W.A., Hameed, I.A., Almuqren, L.A., Raza, M.A., Aslam, M. and Luo, S., 2022. An efficient deep learning-based skin cancer classifier for an imbalanced dataset. *Diagnostics*, *12*(9), p.2115.

[9] Wei, L., Ding, K. and Hu, H., 2020. Automatic skin cancer detection in dermoscopy images based on ensemble

2025

_____

lightweight deep learning network. *IEEE Access*, *8*, pp.99633-99647.

[10] Qasim Gilani, S., Syed, T., Umair, M. and Marques, O., 2023. Skin Cancer Classification Using Deep Spiking Neural Network. *Journal of Digital Imaging*, pp.1-11.

[11] Zhou, Y., Koyuncu, C., Lu, C., Grobholz, R., Katz, I., Madabhushi, A. and Janowczyk, A., 2023. Multi-site cross-organ calibrated deep learning (MuSClD): Automated diagnosis of non-melanoma skin cancer. *Medical image analysis*, *84*, p.102702.

[12] Bassel, A., Abdulkareem, A.B., Alyasseri, Z.A.A., Sani, N.S. and Mohammed, H.J., 2022. Automatic malignant and benign skin cancer classification using a hybrid deep learning approach. *Diagnostics*, *12*(10), p.2472.

[13] Keerthana, D., Venugopal, V., Nath, M.K. and Mishra, M., 2023. Hybrid convolutional neural networks with SVM classifier for classification of skin cancer. *Biomedical Engineering Advances*, *5*, p.100069.

[14] Adla, D., Reddy, G.V.R., Nayak, P. and Karuna, G., 2022. Deep learning-based computer aided diagnosis model for skin cancer detection and classification. *Distributed and Parallel Databases*, *40*(4), pp.717-736.

[15] Khamparia, A., Singh, P.K., Rani, P., Samanta, D., Khanna, A. and Bhushan, B., 2021. An internet of health things-driven deep learning framework for detection and classification of skin cancer using transfer learning. *Transactions on Emerging Telecommunications Technologies*, *32*(7), p.e3963.

[16] Alwakid, G., Gouda, W., Humayun, M. and Sama, N.U., 2022, December. Melanoma detection using deep learning-based classifications. In *Healthcare* (Vol. 10, No. 12, p. 2481). MDPI.

[17] Talasila, S., Rawal, K. and Sethi, G., 2023. Deep Learning-Based Leaf Region Segmentation Using High-Resolution Super HAD CCD and ISOCELL GW1 Sensors. *Journal of Sensors*, *2023*.

[18] Singh, S., Jain, P.K., Sharma, N., Pohit, M. and Roy, S., 2023. Atherosclerotic plaque classification in carotid ultrasound images using machine learning and explainable deep learning. *Intelligent Medicine*.

[19] Yang, X. and Li, S., 2023. Prediction of COVID-19 Using a WOA-BILSTM Model. *Bioengineering*, *10*(8), p.883.

[20] Yang, C., Wang, W., Zhang, X., Guo, Q., Zhu, T. and Ai, Q., 2021, March. A parallel electrical optimized load forecasting method based on quasi-recurrent neural network. In *IOP Conference Series: Earth and Environmental Science* (Vol. 696, No. 1, p. 012040). IOP Publishing.